

Recent in Engineering Science and Technology (RiESTech)

https://www.mbi-journals.com/index.php/riestech

Recent in Engineering Science and Technology (RiESTech), a peer-reviewed quarterly engineering journal, publishes theoretical and experimental high-quality papers to promote engineering and technology's theory and practice. In addition to peer-reviewed original research papers, the Editorial Board welcomes original research reports, state-of-the-art reviews, and communications in the broadly defined field of recent engineering science and technology.

Table of Content Volume 1 Issue 1, 2023

Surface Character of Magnetic Ce-Doped Tio2 for Photocatalytic Performance Enhancement Tia Rahmiati, Ching-Cheng Chen, Siti Asmahani Saad, Nugroho Eko Setijogiarto, Asep Apriana.	1 – 6
Dynotest Design Analysis for Electrical Converted Vehicles Danardono Agus Sumarsono, Fuad Zainuri, Mohammad Adhitya, Muhammad Hidayat Tullah, Rahmat Noval, Sonki Prasetya, Rahmat Subarkah, Tia Rahmiati, Widiyatmoko, Muhammad Ridwan.	7 – 12
Self-Protection Equipment Detection System in Heavy Weight Workshop of Politeknik Negeri Jakarta Using Artificial Intelligence Agus Siswoyo, Eko Aris Cahyonob, Rodik Wahyu Indrawana.	13 – 19
BERSAUDARA Robot (Room And Air Cleaner) As A Prevention Of The Spread of Viruses in Work Areas in Buildings and Isola-Tion Rooms Agus Siswoyo, Eko Aris Cahyono, Rodik Wahyu Indrawan.	20 – 30
Machine Predictive Maintenance by Using Support Vector Machines Idrus Assagaf, Jonri Lomi Ga, Agus Sukandi, Abdul Azis Abdillah, Samsul Arifin.	31 – 35



PT MENCERDASKAN BANGSA INDONESIA (MBI), 4th Floor Gedung STC Senayan Room 31-34, Jl. Asia Afrika Pintu IX, Jakarta 10270, Indonesia.

Indexed by

















Article

Surface Character of Magnetic Ce-doped TiO₂ for Photocatalytic Performance Enhancement

Tia Rahmiati 1*, Ching-Cheng Chen 2, Siti Asmahani Saad 3, Nugroho Eko Setijogiarto 1, Asep Apriana 1

- ¹ Department of Mechanical Engineering, Politeknik Negeri Jakarta, Depok 16424, Indonesia
- ² Department of Materials Science and Engineering, National Dong Hwa University, Hualien 97401, Taiwan
- ³ Department of Civil Engineering, International Islamic University Malaysia, Kuala Lumpur 50728, Malaysia
- * Correspondence: tia.rahmiati@mesin.pnj.ac.id

Abstract: Using a modified sol-gel method for magnetic photocatalyst, the core shell structure of Ce-doped TiO₂@SiO₂@ferrite composite nanoparticles (NPs) was created. X-ray diffraction (XRD), Brunauer–Emmit–Teller (BET), and a superconducting quantum interference device (SQUID) were used to examine the physicochemical properties of the products as they were prepared. The ultraviolet-visible spectrometry (UV-vis) was used to measure the catalyst's photocatalytic activity. On the composite NPs' outer shell coating, the anatase phase related to the TiO₂ structure was constructed. On the Ce-doped TiO₂ layers, a mesoporous structure with uniform pore size was created, resulting in a specific surface area of 111.916 m²g⁻¹. In the meantime, the thin TiO₂ coating contained the redox couple of Ce³⁺ and Ce⁴⁺. An external magnetic field can also be used to separate the catalyst's magnetic NPs from the reaction system. In the aqueous solution of methylene blue (MB), the degradation efficiency and product performance were both 50 percentage.

Keywords: Magnetic photocatalyst; Photodegradation; Cerium doped TiO2; Core shell structure.

Citation: Rahmiati, T.; Chen, C. C.; Saad, S. A.; Setijogiarto, N. G.; Apriana. A.; Surface character of magnetic Ce-doped TiO₂ for photocatalytic performance enhancement. *RiesTech* **2023**, *1*, 4. https://doi.org/00.000/xxxxx

Academic Editor: Iwan Susanto

Received: 17 October 2022 Accepted: 18 November 2022 Published: 1 January 2023

Publisher's Note: MBI stays neutral with regard to jurisdictional claims in published maps and institutional affiliations.



Copyright: © 2023 by the authors. Licensee MBI, Jakarta, Indonesia. This artilcle is an open acess article distributed under MBI license (https://mbi-journals.com/licenses/by/4.0/).

1. Introduction

Organic contaminants and energy crises have been creating serious threats to the environment as globalization and industrialization progress [1, 2]. Semiconductor photocatalysts are a tried-and-true method for converting solar energy into chemical energy to break down pollutants, especially in liquid waste [3, 4]. Due to its excellent photoelectric properties, non-toxic nature, low cost, and high stability, a semiconductor material titanium oxide (TiO₂) has been widely utilized in this system [5–8]. However, the photocatalytic process is hindered in practical applications by the rapid rate of recombination for charge-carrying electron pair holes and the limited range of light response [9, 10]. Numerous attempts have been made to reduce the likelihood of electron hole pair recombination and widen the gap in the TiO₂ absorption band to resolve this issue. Sensitivity design, impurity doping, and integration with other semiconductors are some of the implemented strategies [11–14].

Cerium (Ce) is one of the rare earth elements that has sparked a lot of controversy due to its advantageous properties, which include: 1) the redox couple Ce³⁺/Ce⁴⁺, which facilitates the transfer of photogenerated holes to electron donors, and 2) the straightforward formation of vacancies with a relatively high mobility [15]. Cerium has also been demonstrated to be an effective dopant for increasing the quantum yield in the photocatalytic process by effectively narrowing the band gap and preventing electron-hole recombination [16]. However, the wastewater treatment procedure for separating and manipulating TiO₂ nano composer particles presents yet another issue. Failing to recycle these nanostructures can result in new forms of pollution and also increase the pro-

cessing costs. Nevertheless, due to their unique magnetic response, chemically modified surface, and low cytotoxicity, the include of nano-based magnetic components of TiO₂ particles as catalyst is of particular interest [17]-[19].

As a potential semiconductor photocatalyst material for the degradation of liquid waste from textile dyes, we modify magnetic nanoparticles (NPs) with Ce-coated TiO₂. With Xe arc lamp simulating irradiation of sunlight the aqueous solution of methylene blue (MB) took a role as a model pollutant to carry out the photocatalytic activity. The atomic of TiO₂ with and without doped Ce were the two experimental parameters investigated. Co-doping Ce's potential mechanisms and synergistic effects were thoroughly discussed.

2. Materials and Experiment Methods

2.1 Catalyst synthesis

The tetrabutyltin titanate (Ti(OC4H9)4) that was used to create the final CTSF model was coated with SiO2@ferrite (SF) nanoparticles and doped with 0.5 Ce weight percent. The model was calcined for three hours at 500 °C to produce the anatase phase of TiO2. The sample of F, SF, TSF, and 5CTSF, respectively, were noted for each sample, which included ferrite, SiO2@ferrite, TiO2@SiO2@ferrite, and Ce-TiO2@SiO2@ferrite. To determine the photocatalysts performance and surface structure properties, the samples were further analyzed and tested.

2.2 Catalyst characterization

The crystalline structure observed by X-ray diffraction (XRD) with Cu K radiation (= 0.154056 nm) at a scan rate of 3 °/minutes (Rigaku D/Max-II, Tokyo, Japan). Brunauer–Emmit–Teller (BET) nitrogen adsorption with the Autosorb-1C instrument (Quanta Chrome, Boynton Beach, FL) was used to measure the surface characteristics of surface area, pore volume, and pore size. Adsorbent was nitrogen gas, and the BJH cumulative adsorption method was used to calculate pore volume and size. The superconducting quantum interference device (MPMS5;) was utilized for the ambient temperature measurement of the magnetization properties. With a maximum magnetic field of 10 kOe, the setup (Quantum Design, San Diego, CA) was used.

2.2 Photocatalytic activity

Using a UV–VIS spectrometer (Evolution 220;) and 0.30 g of TSF and 5CTSF magnetic photocatalyst powders in 50 mL of 10 mg/L MB aqueous solution, the concentration of MB was photodegraded. Adsorption–desorption equilibrium prior to the UV illumination process was gained by stirring the suspension for thirty minutes in the darkroom using ultrasonic vibration apparatus. The irradiation function of the TSF and 5CTSF composite was measured under a 35-W Xe arc lamp acting as a simulated sun. Within the duration of six hours, every one hour five milliliters of the suspension were taken, centrifuged, and then analyzed using the MB absorbance intensity at 664.6 nm for powder separation.

3. Results and Discussion

The photocatalyst nanoparticle XRD pattern for the F, SF, and TSF samples is depicted in Figure 1. The XRD pattern of sample F in Figure 2(a) demonstrates the spinel crystal structure of particle ferrite (Ni-Zn). The pattern was consistent with the crystal structure of ferrite Ni-Zn as determined by the Joint Committee of Powder Diffraction Standard (JCPDS), which had the number 08-0234. However, a second phase exist in the pattern, and its JCPDS value was 72-0469 for Fe₂O₃. Additionally, a broader peak pattern suggests that the particles are nanometer sized. The pattern in Figure 1(b) does not contain any SiO₂ peaks after the SiO₂ layer has been deposited. It could be because of the SiO₂ layer's

amorphous structure. Some of the new peaks observed in the XDR pattern in Figure 1(c) can be attributed to the coating of the TiO₂ and Ce-doped TiO₂ on the SF particles. The intensity of some of their previous peaks decreased in tandem with their current one. The anatase phase of TiO₂ gave rise to the new crystal peak at 25.27° in the (101) plane of 2-XRD. The anatase crystal structure of TiO₂ is represented by JCPDS number 21-1272, and the pattern is in line with that. According to the result, the nanoparticle composite of TiO₂@SiO₂@ferrite had a successful TiO₂ layer formed on its outer shell. However, the pattern lacked any Ce peaks, indicating that the entire doping Ce had been incorporated into the TiO₂ crystal structure shown in Figure 2 (b).

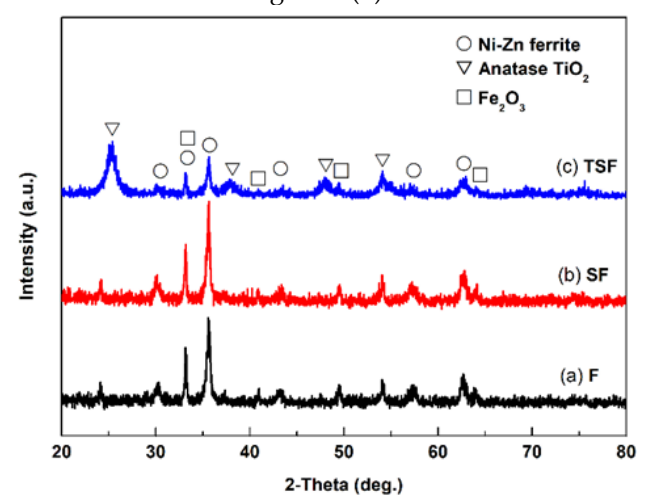


Figure 1. XRD pattern for catalyst particles of (a) F, (b) SF, (c) TSF and (d) 20CTSF

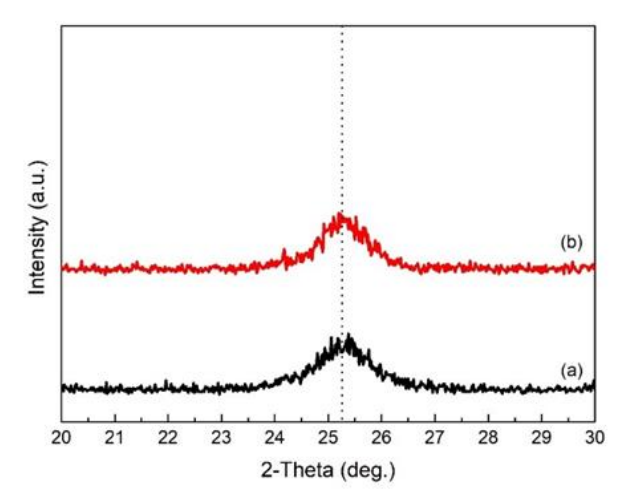


Figure 2. XRD pattern for catalyst particles (a) TSF and (b) 5CTSF between 20 – 30°

The photocatalyst magnetic particles' specific surface area and pore-size distribution were characterized using an adsorption analysis of nitrogen gas. Nitrogen gas isothermal adsorption-desorption for samples F, SF, TSF, and 5CTSF are depicted serially in Figure 3 (a, b, c, and d). For TSF and 5CTSF, the type IV isotherm and H1 type hysteresis loop were investigated, indicating a mesoporous structure of the product. Using the standard multi-points Brunauer-Emmett-Teller (BET) method, the specific surface area (SSA) of the two models was determined to be 126.831 m²g⁻¹ and 135.232 m²g⁻¹, respectively. However, the SSA values for the F and SF models were lower than those for the other two models, as shown in Table 1. The greater the SSA, the more surface contact area could be made possible, which could help speed up the photocatalyst reaction to reduce dye molecules.

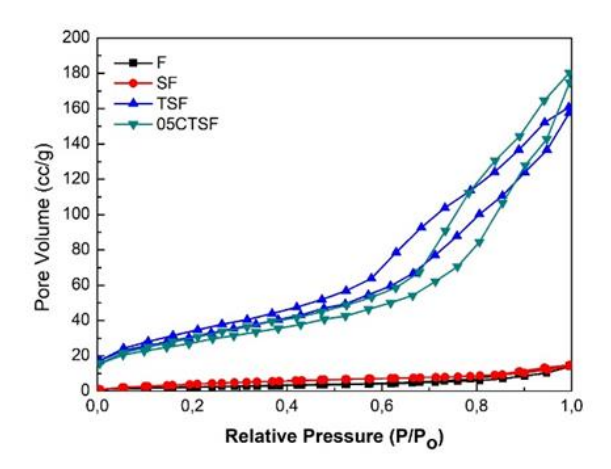


Figure 3. Adsorpsi-desorpsi nitrogen in isothermal for magnetic particle (a)F, (b) SF, (c) TSF, dan (d) 05CTSF

Table 1. The pore characteristic of photocatalyst nanoparticles

Sample	Surface Area SBET (m²/g)	Pore Diameter (Å)	Pore Volume (cc/g)
F	7.586	15.949	0.022
SF	7.395	15.902	0.018
TSF	126.831	26.457	0.244
5CTSF	135.232	28.745	0.345

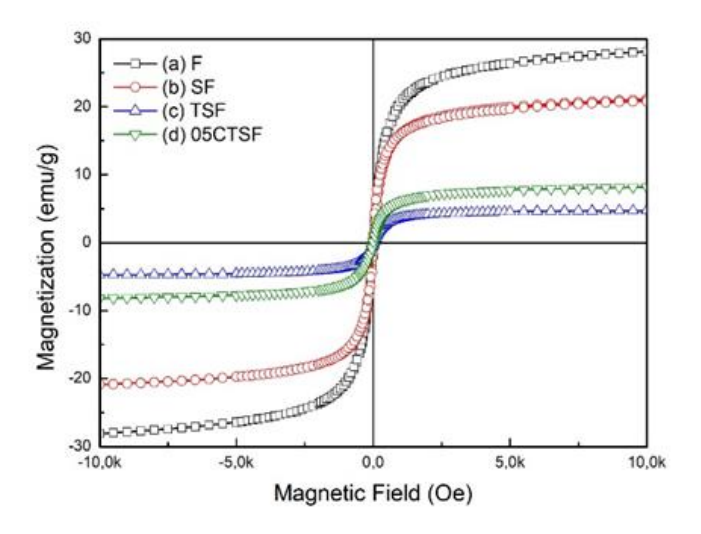


Figure 4. Room-temperature magnetization curve of (a) F, (b) SF, (c) TSF, and 5CTSF composite NPs.

The magnetic curve of magnetic NPs tested at room temperature is shown in Figure 4.F, SF, TSF, and 5CTSF regularly have saturation magnetization values of 28.12, 21.13, 4.73, and 8.25 emu/g, respectively. The value represented the capacity of performance NPs to respond to the magnetic field. The stronger of NPs affected by the magnetic field, the higher the value gained. The minimal hysteresis loop on the magnetization curve of Ni-Zn ferrite indicates a soft magnetic material with a value of 28.12 emu/g, in contrast to

the bulk value of 80 emu/g. Additionally, the nonmagnetic TiO₂ and SiO₂ layer coating over Ni-Zn NPs is responsible for the decreasing saturation magnetization of SF TSF and 5CTSF. The thickness of the shell structure that is formed on the composite magnetic NPs probably influences the lower saturation magnetization. Further, using an external magnetic field from the reaction system, the magnetic NPs can be separated in a magnetic field.

The degradation of MB dye solution under visible light with a 35-watt Xe arch lamp was used to measure the photocatalytic activity of TSF and 5CTSF NPs, as shown in Figure 5. Adsorption-desorption reactions took place in a dark room for 30 minutes prior to photo-degradation under visible light. For TSF and 5CTSF NPs, decolorization of MB dye reached up to 24% and 27%, respectively. It is commonly known that the large surface area and numerous pores of the catalyst NPs in table 1 will make it easier to absorb the dyes in the MB solution. The photodegradation efficiencies were found to be gradually rise within the reaction time as the TSF and 5CTSF NP catalysts were loaded under visible light. In just six hours, the degradation efficiency of the catalyst NPs of TSF and 5CTSF increased from 45% to 55%. It was hypothesized that the redox couple Ce³⁺/Ce⁴⁺ reduced the band gap energy and effective recombination delay of photo-induced charge carriers, resulting in a higher efficiency for the 5CTSF catalyst [15]. It has a useful dopant that increases the quantum yield in the photocatalytic process by enhancing TiO₂'s response [16].

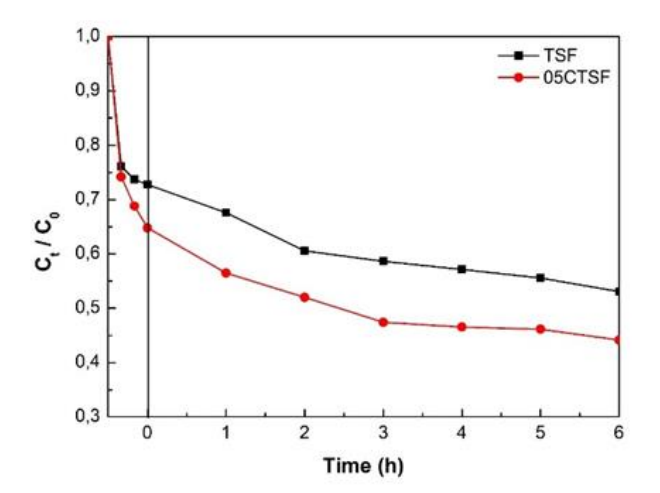


Figure 5. Photodegradation of MB concentration of TSM and 5CTSM NPs composite as a function of irradiation time under visible light, as monitored by changes in the absorbance at 664.6 nm.

4. Conclusions

The magnetic nanoparticles of cerium-doped titanium oxide coated on (Ni-Zn) ferrite NPs as the core were successfully synthesized in this report. On the model's outer core shell structure, the anatase phase of TiO₂ structure has formed. The magnetic core shell NPs have increased pore volume while simultaneously increasing surface area. In addition, a sufficient magnetic field may facilitate the separation of catalyst NPs from the reaction system by an external magnetic field. For Ce-doped TiO₂, the core shell structure's total degradation efficiency reached up 55% after six hours. For MB dye reduction, the performance of catalyst was superior by Ce-doping. The results indicate that the metals transition is one promising option for improving TiO₂'s performance. To maximize the

performance of the photocatalyst for TiO2 NPs, further research was required

Acknowledgments: The authors would like to thank to the research unit and community service of Politeknik Negeri Jakarta for their financial support through the Study Program Leading Research grant in this research.

References

- 1. J. Lei et al., "Ag/AgCl coated polyacrylonitrile nanofiber membranes: Synthesis and photocatalytic properties," React. Funct. Polym., vol. 71, no. 11, pp. 1071–1076, 2011.
- 2. J. Zhang, B. Tian, L. Wang, M. Xing, and J. Lei, Photocatalysis. Singapore: Springer US, 2018.
- 3. D. V. Bavykin, J. M. Friedrich, and F. C. Walsh, "Protonated titanates and TiO2 nanostructured materials: Synthesis, properties, and applications," Adv. Mater., vol. 18, no. 21, pp. 2807–2824, 2006.
- Q. Zhang, D. Q. Lima, I. Lee, F. Zaera, M. Chi, and Y. Yin, "A highly active titanium dioxide based visible-light photocatalyst with nonmetal doping and plasmonic metal decoration," Angew. Chemie - Int. Ed., vol. 50, no. 31, pp. 7088–7092, 2011.
- R. Li, H. Kobayashi, J. Guo, and J. Fan, "Visible-light-driven surface reconstruction of mesoporous TiO2: Toward visible-light absorption and enhanced photocatalytic activities," Chem. Commun., vol. 47, no. 30, pp. 8584–8586, 2011. Title of Site. Available online: URL (accessed on Day Month Year).
- 6. Y. Zhao, Y. Wang, G. Xiao, and H. Su, "Fabrication of biomaterial/TiO 2 composite photocatalysts for the selective removal of trace environmental pollutants," Chinese J. Chem. Eng., p. #pagerange#, 2019.
- 7. Z. Xing et al., Recent advances in floating TiO2-based photocatalysts for environmental application, vol. 225. Elsevier B.V., 2018.
- 8. Y. Wang et al., "The Application of Nano-TiO2 Photo Semiconductors in Agriculture," Nanoscale Res. Lett., vol. 11, no. 1, pp. 1–7, 2016.
- 9. L. L. Tan, S. P. Chai, and A. R. Mohamed, "Synthesis and applications of graphene-based TiO2 photocatalysts," ChemSusChem, vol. 5, no. 10, pp. 1868–1882, 2012.
- K. Ozawa et al., "Electron-Hole Recombination Time at TiO2 Single-Crystal Surfaces: Influence of Surface Band Bending," J. Phys. Chem. Lett., vol. 5, no. 11, pp. 1953–1957, 2014.
- 11. V. Subramanian, E. E. Wolf, and P. V. Kamat, "Catalysis with TiO2/Gold Nanocomposites. Effect of Metal Particle Size on the Fermi Level Equilibration," J. Am. Chem. Soc., vol. 126, no. 15, pp. 4943–4950, 2004.
- 12. F. Chen et al., "Fabrication of Fe3O4@SiO2@TiO2 nanoparticles supported by graphene oxide sheets for the repeated adsorption and photocatalytic degradation of rhodamine B under UV irradiation," Dalt. Trans., vol. 43, no. 36, pp. 13537–13544, 2014.
- 13. J. H. Park, S. Kim, and A. J. Bard, "Novel carbon-doped TiO 2 nanotube arrays with high aspect ratios for efficient solar water splitting," Nano Lett., vol. 6, no. 1, pp. 24–28, 2006.
- 14. W. L. Ong, M. Gao, and G. W. Ho, "Hybrid organic PVDF-inorganic M-rGO-TiO2 (M = Ag, Pt) nanocomposites for multifunctional volatile organic compound sensing and photocatalytic degradation-H2 production," Nanoscale, vol. 5, no. 22, pp. 11283–11290, 2013.
- 15. T. Yu, X. Tan, L. Zhao, Y. Yin, P. Chen, and J. Wei, "Characterization, activity and kinetics of a visible light driven photocatalyst: Cerium and nitrogen co-doped TiO2 nanoparticles," Chem. Eng. J., vol. 157, no. 1, pp. 86–92, 2010.
- 16. I. Tbessi et al., "Effect of Ce and Mn co-doping on photocatalytic performance of sol-gel TiO2," Solid State Sci., vol. 88, pp. 20–28, 2019.
- 17. C. C. Chen, Y. P. Fu, and S. H. Hu, "Characterizations of TiO2/SiO2/Ni-Cu-Zn Ferrite Composite for Magnetic Photocatalysts," J. Am. Ceram. Soc., vol. 98, no. 9, pp. 2803–2811, 2015.

Article

Dynotest Design Analysis for Electrical Converted Vehicles

Danardono Agus Sumarsono ^{1*}, Fuad Zainuri ^{2,3}, Mohammad Adhitya ¹, Muhammad Hidayat Tullah ^{1,2,3}, Rahmat Noval ^{1,3}, Sonki Prasetya ^{2,3}, Rahmat Subarkah ^{2,3}, Tia Rahmiati ², Widiyatmoko ³, Muhammad Ridwan ^{2,3}

- ¹ Department of Mechanical Engineering, Universitas Indonesia, Depok 16424, Indonesia
- ² Department of Mechanical Engineering, Politeknik Negeri Jakarta, Depok 16425, Indonesia
- ³ Center of Automotive (CoA), Politeknik Negeri Jakarta, Depok 16425, Indonesia
- * Correspondence: fuad.zainuri@mesin.pnj.ac.id

Abstract: The study comprises dynotest design and analysis to measure torque and horsepower. Basically, a dynotest carried out by apply certain load to the axle of a combustion motor through the braking mechanism of its crankshaft. Due to the high price of a Dynotest unit in the market, it is relatively difficult for a developing institution to own it on their site. The study target to design a simple and good accurate Dynotest within a reasonable price. The study used a common standard method for design analysis which rely on function and structural approach. Functionally, Dynotest is designed to be used to an ouput of an electical motor. Loading on motor shaft was done by disc brake braking mechanism. Structurally, Dynotest was designed to use rollers. As a main component, its mounting construction is connected to a motor to generate electrical power. Power transmitted from the motor to Dynotest through a center joint shaft, torque measured by load cell while the rotation of shaft itself counted by a digital tachometer. Test result show that electricity was produced from the simple construction and Dynotest functioned well in measuring it. Measurement data of roller support shaft performance showed a motor torque performance curve which are similar with the typical of similar Dynotest. Construction Test done by applying Solid Work software analysis to some components partially on rollers and on the construction assembly as a whole unit.

Keywords: Roller; Dynotest; Listrik; Assembly.

Citation: Sumarsono, D. A.; Zainuri, F.; Adhitya, M.; Tullah, M. H.; Noval, R.; Prasetya, S.; Subarkah, R.; Rahmiati, T., Widiatmoko, M.; Ridwan, R. Dynotest Design Analysis for Electrical Converted Vehicles. *RiesTech* 2023, 1, 5. https://doi.org/00.000/xxxxx

Academic Editor: Iwan Susanto

Received: 3 October 2022 Accepted: 28 November 2022 Published: 1 January 2023

Publisher's Note: MBI stays neutral with regard to jurisdictional claims in published maps and institutional affiliations.



Copyright: © 2023 by the authors. Licensee MBI, Jakarta, Indonesia. This article is an open acess article distributed under MBI license (https://mbi-

journals.com/licenses/by/4.0/).

1. Introduction

Officially stated in RUEN (Rencana Umum Energi Nasional/General Planning of National Energy) 2020, Indonesia targets to build 2.200 unit of electric/hybrid 4 wheels vehicles dan 2.1 million unit of those in 2025. This RUEN is a continuance of Peraturan Presiden (PER-PRES) Nomor 55 Tahun 2019 [1]. "Percepatan Program Kendaraan Bermotor Listrik Berbasis Baterai (Battery Electric Vehicle) untuk Transportasi Jalan.

The national position of our research itself is now to continue the conversion program to have an electric vehicle with manual transmission, which is more user-friendly and effective in urban surroundings [2]. Already achieved the most suitable gear ratio to fit a transmission system for a certain speed. Further analysis has been taken to find the optimum motor performance in serving various field [3]. Classically we knew that there are efficiencies among components in a conventional vehicle, such as transmission, axle, and differential, but in an EV (electrical vehicle) the efficiency of a transmission unit is regarded ideal even constant [4]. An EV performance is calculated by its speed and working threshold variables, which are rolling resistance, air friction coefficient, gradient resistance also its inertia [5].

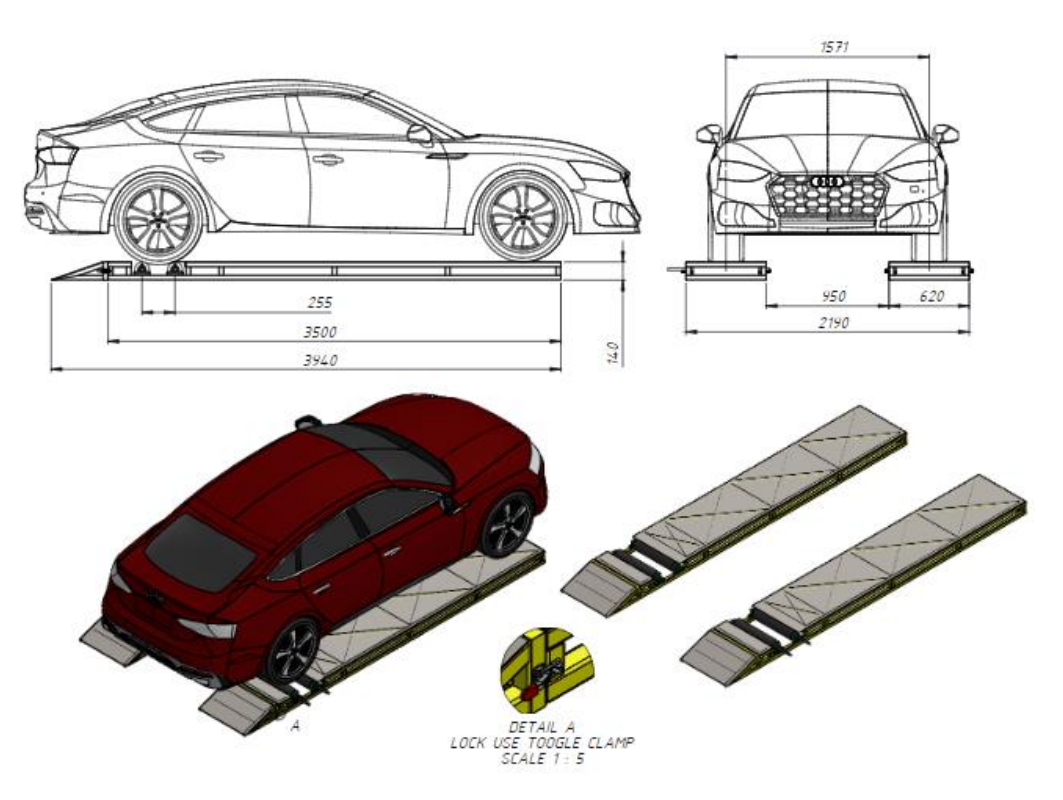


Figure 1. Design Model of Dynotest Unit [7]

Characteristics of a motor represented by a chart describing the relation between power, torque etc versus rpm of a constant throttle openings. There we can plot the traction force (Pt) vs vehicle speed of some certain speed rates. Then we can determine the torque value for certain rpm by using Eq. 1 [8].

T = 9549 (1) where: T is the Torque of the motor (N m) N is Work of the motor (kW) in (rpm)

Dynotest is a measuring tool for torque result and horsepower. In advance automotive fields, many major companies apply the test in its manufacturing. The machinery will always grow and develop every time and there will always efforts to improve performance of components in many aspects such as speed, comfortability and cost savings. A torque and horsepower of a machine can be easily calculated by a dynotest apparatus. [3].

The scope of the study was to perform a series of dynotest of a converted EV through the measurement of rpm, torque, and horsepower of its prime mover motor. The test done under different gear positions so that from torque and horsepower data gained the optimal conditions of every position can be plotted. The test revealed some areas where gear shipment did not trigger a deceleration and promoted a motor efficiency in an EV [8]. Research development and modelling that have been done in the study can be utilized further to have more effective and efficient value.

2. Materials and Experiment Methods

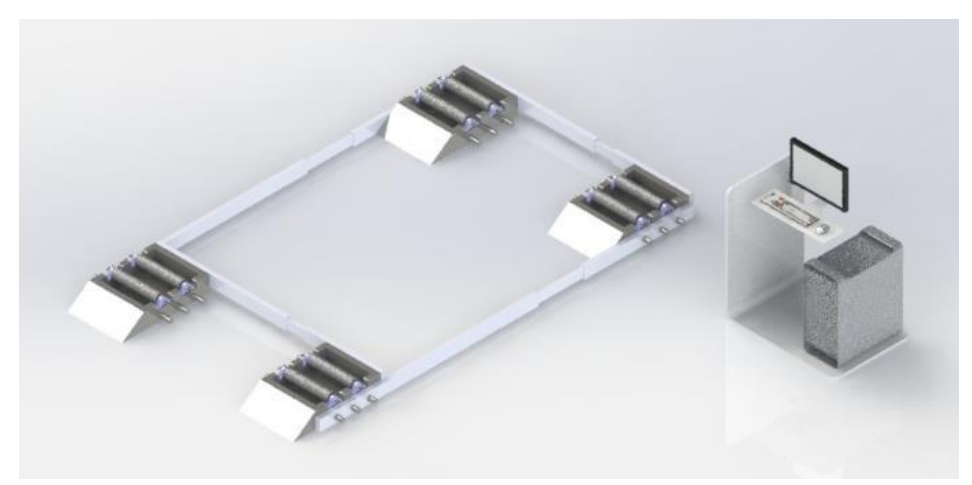


Figure 2. Dynotest installation unit

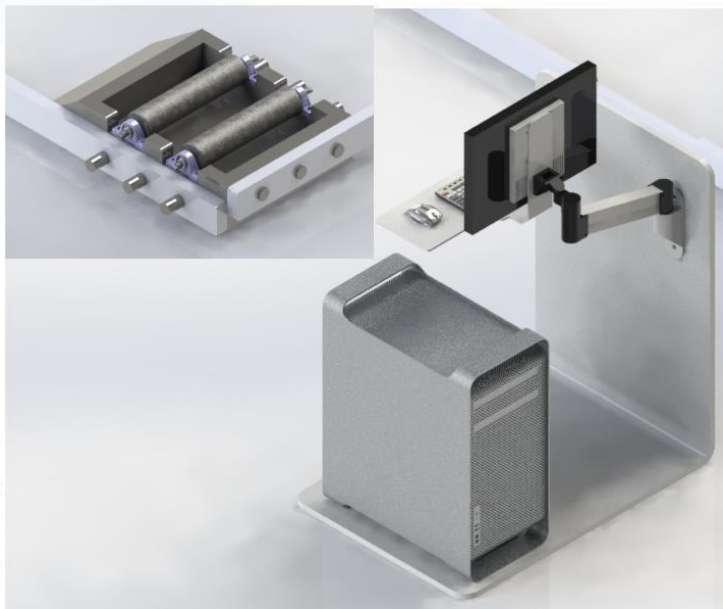


Figure 3. Dynotest Installation

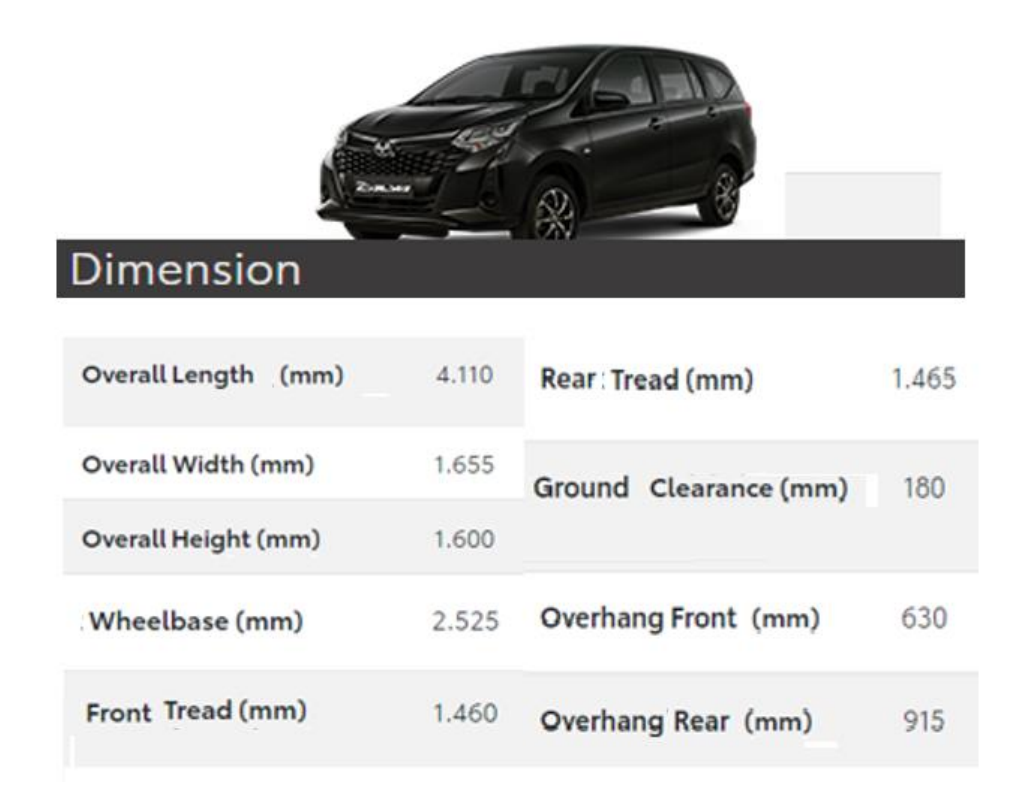
Followings are steps in collecting data of torque and horsepower result. Initially the dynotest unit have to be calibrated within braked condition. Mark the value in multimeter used as a reference reading. After calibrated, put the vehicle on the dynotest chassis.

Due to too much equipment's installed and all must work in one integration without room of failure, prior to the test partially the system itself has to be tested. This to ensure every part functioned well before interface it with the others. Test the EV unit on the planned parameters. The phase of integration, improvement and testing are the longest phases, actually unlimited for the improvement of EV in Indonesia. The result of any study will be a good startup for developing further.

Speed of the test is decided as 80 km/hour. The speed is become the profile for a converted EV with the specification frontal area approximately 4.16m2, aerodynamic friction (Cd) 0.5328 and rolling friction 0.002. The vehicle was tested without passenger load and

without activating secondary function, therefore only main motor is switched on. An EV is driven by 1 (one) main 3 phase motor.

Tabel .1 Test Vehicle Specification



3. Results and Discussion

Data Analyze of Dynotest Software Simulation.

Horsepower measurement (HP) of each speed condition and each gear reveal that the value of HP of 1^{st} gear has lower resistance than those of the 5^{th} gear, with the biggest resistance held by 4^{th} gear. Torque measurement of each speed also showed that the torque when 1^{st} gear is applied, is lower than the torque when 5^{th} is applied. Optimum condition reached when 4^{th} gear is used.

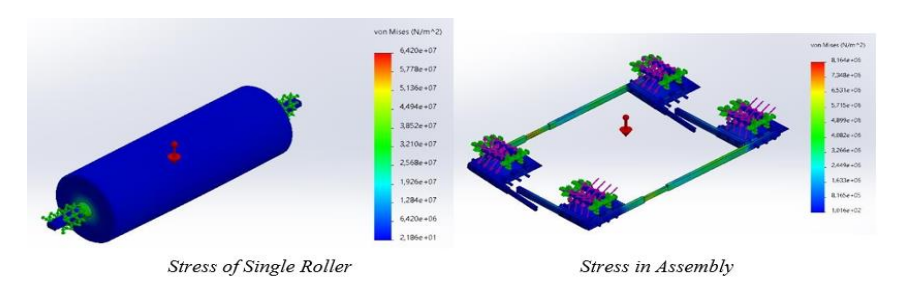


Figure 4. Stress Analysis

Figures above describe stress analysis of a dyno test machine. The left is the stress distribution of a roller while the right one is the stress analysis of a complete set of dyno assembly. There are 4 (four) color: blue, green, yellow and red. Blue represent the lowest stress while red the highest one.

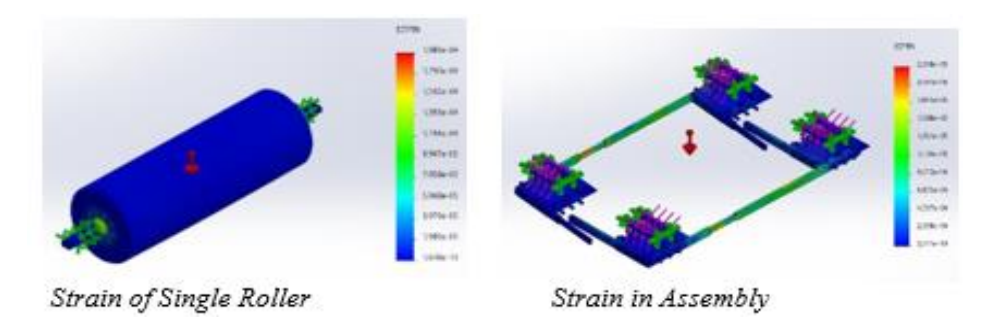


Figure 5. Strain Analysis

With the same color configuration, Figure 5 representing strain analysis. Area with biggest strain is the roller shaft (left) and the roller bar connectors (right)

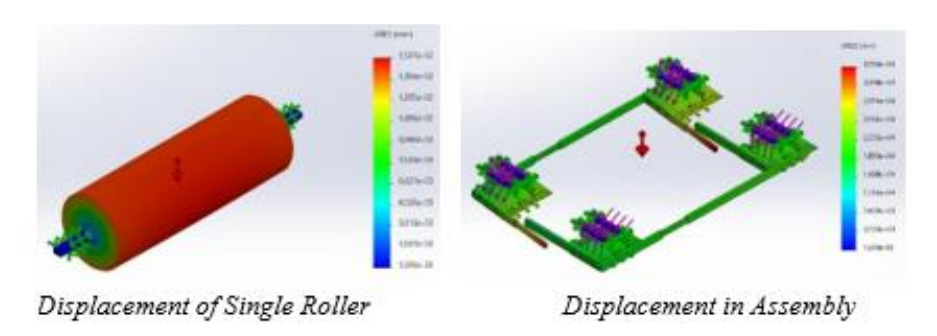
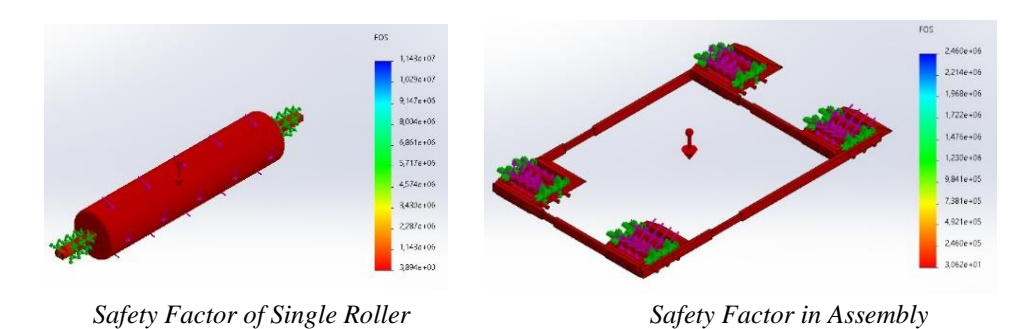


Figure 6. Displacement Analysis

The biggest displacement is the surface of single roller (left drawing), front connector for assembly.



Gambar 7. Safety Factor Analysis

Safety factor value of 3,89e+00 single roller and 3,062e+01 for the assembly, signify the dyno test machine is safe to be fabricated. For the optimum, there are 2 possibilities by applying 2 (two) gear combination to have optimum set of horsepower, torque, and rpm.

4. Conclusions

- Need a sustainable regeneration to have a continuance of the research.
- Combination of speed, acceleration, deceleration also kerbs will give different phenomenon of force produced.
- Theoretically, the average output is higher than the average of actual input of a motor. This should be investigated in a further study.
- The study, research, improvement, and development of EV is a very strategic to continue.

Acknowledgments:

Warm and big gratitude and respect of the author to UP2M PNJ, RCAVe UI and Ristek Brin Dirjen Dikti and Vokasi who support the article's writings.

References

- 1. M. Adhitya Ect., "Development a New Model of Synchromesh Mechanism to optimization Manual Transmission's Electric Vehicle," p. 2018, 2018.
- 2. D. A. S. G Heryana, S Prasetya, M Adhitya, "Power consumption analysis on large-sized electric bus," IOP Conf.Ser. Earth Env., vol. 105, no. 012041, 2018.
- 3. T. Shi, F. Zhao, H. Hao, and Z. Liu, "Development Trends of Transmissions for Hybrid Electric Vehicles Using an Optimized Energy Management Strategy," Automot. Innov., vol. 1, no. 4, pp. 291–299, 2018, doi: 10.1007/s42154-018-0037-5.
- J. Michaelis, T. Gnann, and A. L. Klingler, "Load shifting potentials of plug-in electric vehicles-A case study for Germany," World Electr. Veh. J., vol. 9, no. 2, 2018, doi: 10.3390/wevj9020021.
- R. Siregar, U. D. Persada, D. A. Sumarsono, and F. Zainuri, "Design a New Generation of Synchromesh Mechanism to Optimization Manual Transmission's Electric Vehicle," 15th Int. Conf. QIR, no. May 2019.
- M. Rozman et al., "Smart Wireless Power Transmission System for Autonomous EV Charging," IEEE Access, vol. 7, pp. 112240–112248, 2019, doi: 10.1109/access.2019.2912931.
- 7. F. Zainuri, D. A. Sumarsono, M. Adhitya, and R. Siregar, "vehicle Design of Synchromesh Mechanism To Optimization Manual Transmission's Electric Vehicle," AIP Cpublishing Conf. Pros., vol. 020031, 2017, doi: 10.1063/1.4978104.
- 8. M. R. Ahssan, M. M. Ektesabi, and S. A. Gorji, "Electric Vehicle with Multi-Speed Transmission: A Review on Performances and Complexities," SAE Int. J. Altern. Powertrains, vol. 7, no. 2, 2018, doi:10.4271/08-07-02-0011.

Article

Self-Protection Equipment Detection System in Heavy Weight Workshop of Politeknik Negeri Jakarta Using Artificial Intelligence

Muhammad Reza Kusuma ¹, Abdul Azis Abdillah ^{1*}, Dewi Yanti Liliana ², Ega Edistria ³, Samsul Arifin ⁴, Zahran Muzakki ⁵

- ¹ Department of Mechanical Engineering, Politeknik Negeri Jakarta, Depok 16425, Indonesia
- $^{2} \quad \text{Department of Informatics and Computer Engineering, Politeknik Negeri Jakarta, Depok 16425, Indonesia}$
- ³ Department of Civil Engineering, Politeknik Negeri Jakarta, Depok 16425, Indonesia
- ⁴ Department of Mathematic, Universitas Bina Nusantara, Indonesia
- ⁵ PT Tochterindo Prima Persada, Indonesia
- * Correspondence: abdul.azis.a@mesin.pnj.ac.id

Abstract: The creating process, how it works and the performance of the detection system using Artificial Intelligence. The development of this innovation contributes to the Heavy Equipment Workshop of the Jakarta State Polytechnic to detect the early potential for work accidents. The methods are device tuning, inputs, training models, performance, trials and outputs. The creating process and how the detection system works using Artificial Intelligence each has 3 steps and accuracy using 3 cameras, namely the internal webcam (1MP), the JETE external webcam (720P) and the Samsung Galaxy A22 mobile phone camera (13MP). The process of making this innovation has 3 steps, namely data input, export, file grouping. There are 3 steps to work, namely open the file, run and output. The result of the accuracy of the internal webcam is very low, the JETE external webcam is better than the internal webcam and the mobile phone camera is better than the JETE external webcam.

Keywords: Detection system; Artificial intelligence; Input; Performance.

Citation: Kusuma, M. R.; Abdillah, A. A.; Liliana, D. Y.; Edistria, E.; Arifin, S.; Muzakki, Z.
Self-Protection Equiptment Detection System in Heavy Weight
Workshop of Politeknik Negeri
Jakarta Using Artificial Intel-ligence.
RiesTech 2023, 1, 1.
https://doi.org/00.000/xxxxx

Academic Editor: Iwan Susanto

Received: 5 September 2022 Accepted: 1 November 2022 Published: 1 January 2023

Publisher's Note: MBI stays neutral with regard to jurisdictional claims in published maps and institutional affiliations.



Copyright: © 2023 by the authors. Licensee MBI, Jakarta, Indonesia. This artilcle is an open acess article distributed under MBI license (https://mbi-journals.com/licenses/by /4.0/).

1. Introduction

Work Accident are unplanned and unpredictable events in every company. In a large company or small one, it has to be reduced to a minimum. Work accident is an unwanted event in a certain work area, happened due to dangerous act and dangerous condition (Nur, 2019).

Data from BPJS Ketenagakerjaan reveals in 2017 work accidents reached 123.041 cases, while 2018 reached 173.105 cases, and at the end of 2021 the number is about 82.000 cases. Work accident is caused by 2 factors: unsafe act and unsafe condition. Work accident effects both on company and the workers. The company suffers on productivity and ability decrease, higher operational cost, machinery and properties breakdown, product deterioration. On the other hands, workers suffer major and minor injury, physical disability even fatality. Lack of supervision on K3 (Keselamatan dan Kesehatan Kerja, basic working safety and health condition) also contributes to the work accident occurrences. It is obvious that the performance done by human in supervision will decrease along

with time, so therefore the necessity of automation technology help is surfacing up as an ultimate solution.

In 4.0 industry era, Artificial Intelligence (A.I.) give a promising satisfactory solution. The automation system made is able to detect workers in 24/7 of K3, so that the potentiality of working accident can be early detected.

2. Materials and Experiment Methods

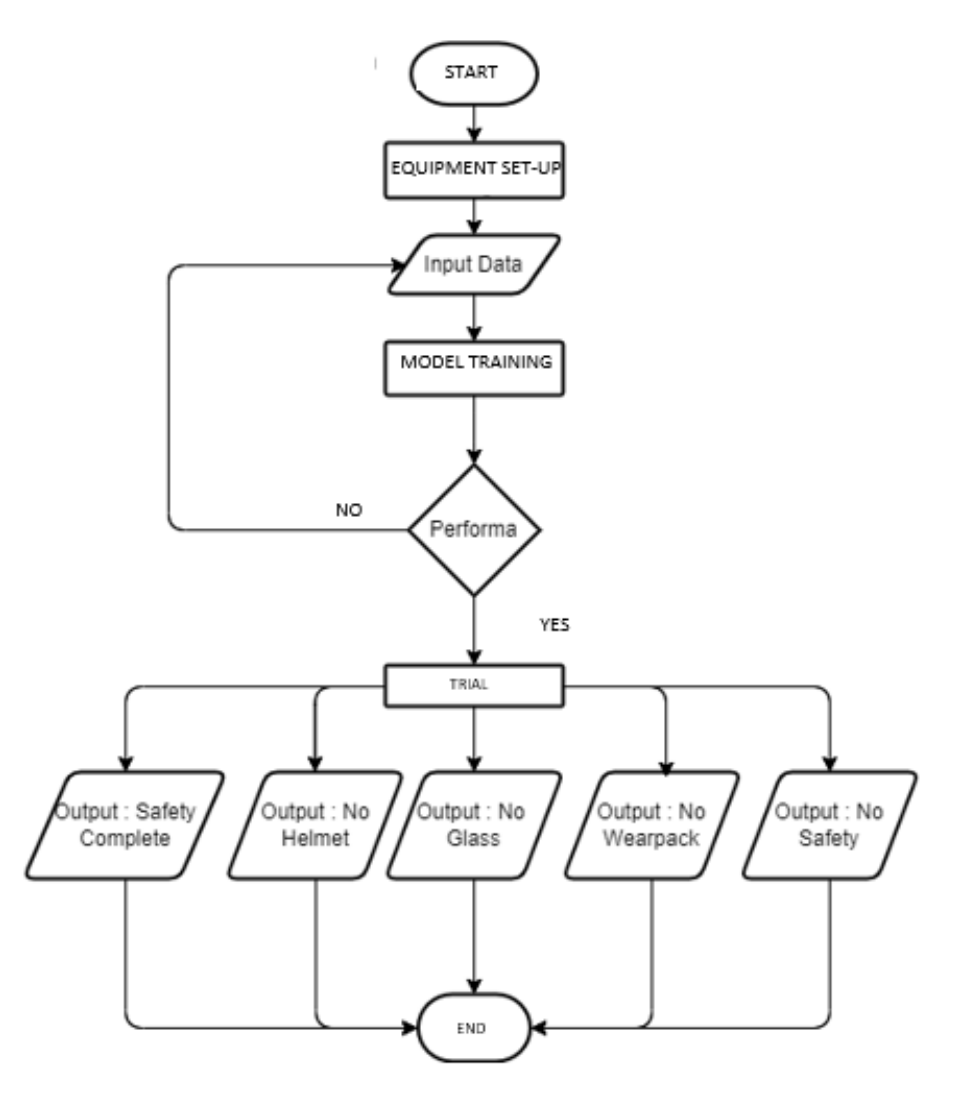


Figure 1. Flowchart.

Flow chart description:

A. Equipment set-up

The equipment set up done by connecting the computer with the mouse and external webcam. Open then the software Teachable Machine inside the computer and aim for the body part that will be captured.

B. Input Data

Data input is an activity of data key-in to be a set of reference model. Data input quantity needed will be range from 1000 to 1100. The photo taken comprises 5 (five) major condition:

Table 1. Data Condition.

No	Condition			
1	The photo of all the personal protective equiptment worn			
2	Photo without safety helmet.			
3	Photo without safety glasses.			
4	Photo without safety outfit.			
5	The photo without wearing all protective equiptment worn.			

C. Modelling

Data input will be processed and calibrated by Teachable Machine website. There site system will be processed and calibrated into codes.

D. Performance Measurement

Accuracy Measurement Method used is in format of Intersection over Union (IoU) range 0,01 until 1,00. Teachable Machine convert the decimal into percentage format. The lowest percentage is 50% (Kristal and Harintaka 2022). If below 50% it requires re-input the data.

E. Trial Experimentation Period

After the performance reached 50%, the model then exported onto a folder which will be downloaded the computer. The trial experimentation period then will be commenced by re-running the model using Visual Studio Code software and Python 3.8.6.

F. Output

Trial result in the text output format. Output read by the system will be:

Table 2. Output and Condition

Code	Output	Condition	
0	Safety Complete	Wear all the self safety protective equiptment	
1	No Helmet	Not wearing safety helmet	
2	No Glass	Not wearing safety glasses	
3	No Wearpack	Not wearing safety uniform	
4	No Safety	Not wearing all self safety protective equiptment	

3. Results and Discussion

Performance comparation tested by using some various camera and viewpoints.

Webcam Internal

Webcam Internal is the default camera installed on the computer. In this article Samsung ATIV Book with front camera 1MP s used.



Figure 2. Output Webcam Internal.

When webcam internal used, the output value is not changing. It shows 0% constantly.

Code	Output	Detected Value
0	Safety Complete	0
1	No Helmet	0
2	No Glass	0
3	No Wearpack	0
4	No Safety	0
	TOTAL	
PERCENTAGE		0%

Table 3. Webcam Internal.

Two things became the main cause possibilities of the problem. First: the camera specification is too low. Secondly: the existing code will not be able to run the camera to detect motion.

A. Webcam External

External webcam JETE W5 Series (picture resolution 720P) used. The result is far more different and better. The motion is detectable and 60% accuracy value is achieved.



Figure 3. Output Webcam External.

Table 4. External Webcam Percentage Result.

Code	Output	Detected Value
0	Safety Complete	1
1	1 No Helmet 0	
2	No Glass 1	
3	No Wearpack	0
4	No Safety	1
TOTAL		3
PE	RCENTAGE	60%

B. Cellphone Camera

Cellphone Camera Samsung Galaxy A22 with the front camera specification 13MP also utilized and the accuracy value reached 80%.



Figure 4. Output Kamera Handphone.

Gambar 4. Cellphone Camera result.

Table 5. Cellphone Camera.

Code	Output	Detected Value
0	Safety Complete	1
1	No Helmet	0
2	No Glass	1
3	No Wearpack	1
4	No Safety	1
TOTAL		4
PERCENTAGE		80%

4. Conclusions

The accuracy of detection system using AI is vary depend of the camera used. The variations are as follows:

- 1. Webcam internal computer Samsung ATIV Book 2 1MP. Accuracy percentage value 0%.
- 2. Webcam external JETE W5 Series 720P achieved accuracy value 60%.
- 3. Front camera Samsung Galaxy A22 13MP The accuracy value best achieved 80%.

Concluded the better camera resolution used the far more good result in accuracy value is achieved in the detection system.

References

- 1. Jeong, Hyunja. 2020. "Feasibility Study of Google's Teachable Machine in Diagnosis of Tooth-Marked Tongue.". Journal of Dental Hygiene Science 20(4): 206–12.
- 2. Jaya, Hendra et al. 2018. 53 Journal of Chemical Information and Modeling Kecerdasan Buatan.

- 3. Kristal, Agri, and Harintaka Harintaka. 2022. "Analisis Kehandalan Ekstraksi Garis Tepi Bangunan Dari Data Foto Udara Menggunakan Pendekatan Deep Learning Berbasis Mask R-CNN." Geoid 17(2): 273.
- 4. Mulyawan, Hendy, M Zen Hadi Samsono, and Setiawardhana. 2011. "Identifikasi Dan Tracking Objek Berbasis Image.": 1–5. http://repo.pens.ac.id/1324/1/Paper_TA_MBAH.pdf.
- Nur, Muhammad. 2019. "ANALISIS KECELAKAAN KERJA DENGAN MENGGUNAKAN METODE HAZARD AND OPERABILITY STUDY (HAZOP) (Studi Kasus: PT. XYZ)." Jurnal Teknik Industri Terintegrasi 2(2): 30–37.
- 6. Welim, Yohannes Yahya, Wisjhnuadji T.W., and Rasip Firmansyah. 2015. "Pengembangan Sistem Informasi Service Kendaraan Pada Bengkel Kfmp." Simetris: Jurnal Teknik Mesin, Elektro dan Ilmu Komputer 6(1): 17.
- 7. Ismara, K.I, Nuha, Eko. 2020. "Bekerja Dengan Alat Berat Secara Selamat dan Sehat". Yogya-karta. UNY Press.
- 8. Salamah, U.G. 2021. "Tutorial Visual Studio Code." Bandung. CV. Media Sains Indonesia
- Menteri Tenaga Kerja dan Transmigrasi. 2010. "Peraturan Menteri Tenaga Kerja Dan Transmigrasi Republik Indonesia." Peraturan Menteri tenaga Kerja dan Transmigrasi VII (8): 1–69. https://indolabourdatabase.files.wordpress.com/2018/03/permenaker-no-8-tahun-2010-tentangapd.pdf.

Article

BERSAUDARA Robot (Room and Air cleaner) as a prevention of the spread of viruses in work areas in buildings and isolation rooms

Agus Siswoyo 1*, Eko Aris Cahyono 2, Rodik Wahyu Indrawan 1,2

- Department of Mechatronics, Universitas Sanata Dharma, Sleman, Indonesia
- ² Department of Robotics and Artificial Intelligence Engineering, Universitas Airlangga, Surabaya, Indonesia
- Correspondence: woyo@usd.ac.id

Abstract: BERSAUDARA Robot innovation emerged based on health protocols in the new normal era and workers' anxiety about the spread of viruses in buildings. This robot is designed by utilizing the development of robotics technology, Remote Operated Vehicle (ROV), vacuum floor cleaner, and air purifier equipped with UV Sterilizer and HEPA Filter. BERSAUDARA Robot innovation is expected to fulfill the protocol for preventing the spread of the Covid-19 virus, especially work areas in buildings or isolation rooms, by cleaning floors and air regularly so as to minimize human contact and support the continuity of the activities of workers during the "New Normal".

Keyword: Mobile Robot; Remote Operated Vehicle (ROV); Covid-19; Hepa filter.

1. Introduction

Coronavirus Disease 2019 (COVID-19) is a new type of disease that has never been previously identified in humans. The virus that causes COVID-19 is called Sars-CoV-2. On January 30, 2020 WHO has declared it a Public Health Emergency of International Concern (KKMMD/PHEIC) [1]. This virus was identified as being able to transmit from human to human through droplets, infecting all ages. In particular, humans with weakened immune systems have a higher risk of infection.

As an effort to prevent the spread of the COVID-19 virus, the government has made a handling program, one of which are health protocols starting from wearing masks, diligently washing hands, always keeping a distance to avoid physical contact and guidelines for activities during the new normal order or "New Normal". The Minister of Health of the Republic of Indonesia Number HK.01.07/MENKES/328/2020 for the prevention of transmission in the work area has also provided guidance on pandemic situations, namely providing safe and healthy workplace facilities, regular cleaning, appropriate disinfectants (every 4 hours), and maintain workplace air quality by optimizing air circulation. The activities of managing cleanliness and sanitation of work areas in buildings or isolation rooms are currently still carried out manually with limited personal protective equipment and lack of availability of air. circulation, especially in areas within the building, thus creating a risk of spreading transmission to officers and workers who are active in the building.

BERSAUDARA Robot innovation emerged on health protocols regulations in the new normal era and from workers' anxiety about the spread of viruses in buildings. This robot is designed by utilizing the recent development of robotics technology, Remote Op-

Citation: Siswoyo, A.; Cahyono E. A.; Indrawan, R. W. BERSAUDARA Robot (Room and Air cleaner) as a prevention of the spread of viruses in work areas in buildings and isolation rooms. RiesTech 2023, 1, 3. https://doi.org/00.000/xxxxx

Academic Editor: Iwan Susanto

Received: 16 September 2022 Accepted: 14 November 2022 Published: 1 January 2023

Publisher's Note: MBI stays neutral with regard to jurisdictional claims in published maps and institutional affiliations



Copyright: © 2023 by the authors. Licensee MBI, Jakarta, Indonesia. This article is an open acess article distributed under MBI license (https://mbi-

journals.com/licenses/by/4.0/).

erated Vehicle (ROV), vacuum floor cleaner, and air purifier equipped with UV Sterilizer and HEPA Filter. The stages in making the robot begin with design planning, initial testing, stage I validation, stage II validation, and the implementation. BERSAUDARA Robot innovation is expected to fulfil the protocol of preventing the spread of the Covid-19 virus, especially in work areas of buildings or isolation rooms, by cleaning floors and air regularly so as to minimize human contact and support the continuity of the activities of workers during the "New Normal". This research is also in line with the objectives of the 2016-2020 Sanata Dharma University Research Master Plan, which is to develop knowledge, produce innovations that are able to solve independent and sustainable problems for the community, and be proactive in the demands of strategic environmental developments.

2. Materials and Experiment Methods

A. Analysis

Sensor for mapping, localization, and navigation of mobile robots rely heavily on available information about the state of the robot and the environment. Typical sensors for mapping are:

- The odometry is usually calculated from the measurements of the encoder mounted on the wheel. It can estimate the displacement of the robot, but the accumulation of errors makes its application unfeasible, as a unique source of information, in real applications.
- 2. GPS (Global Positioning System) is a good option outdoors, but loses its capability near buildings, on narrow streets, and indoors.
- 3. SONAR (Sound Navigation and Ranging) allows measurement of the distance to objects located in the vicinity, through the emission of sound pulses and measurement of the reception of echoes from these pulses. However, the precision is relatively low, as it tends to present high angle uncertainty and some noise caused by reflected sound signals.
- 4. The laser sensor determines the distance by measuring the flight time of the laser pulse as it bounces off a neighboring object. Their precision is higher than that of SONAR, and they can measure distances from centimeters to tens of meters with relatively good angular precision and resolution.

B. Design

BERSAUDARA robot is designed to have an omnidirectional movement mechanism so that it can walk in every corner of the workplace or isolation room, this robot is equipped with a remote-control system, floor cleaner, and air purifier.



Figure 1. Design BERSAUDARA robot



Figure 2. Design BERSAUDARA robot

The mechanical design of this robot supports it's ability to move in the terrain. The material components of the robot use aluminum for both the base and it's upper body construction. Aluminum was chosen because it is relatively easy to adjust/form and its lightweight gives an advantage when the robot is maneuvering in a narrow room.

C. Development

Map Building and Subsequent Localization

Solving the localization problem requires a pre-built environmental model, so that the robot is able to position and route itself by comparing its sensory information with the information captured in the model.

This robot itself is a development of a prototype automated guided vehicle, which is useful for Covid-19 hospitals. The tools attached in the robot was equipped and developed to assist and solve air and air problems. The tool is controlled using a Cytron ps2 remote with visuals captured by the DDPAI camera. The microcontroller system activates Mega 2560, this is to activate three IBT-2 to lift or run the PG45 motor and one DC relay to trigger the switch from the vacuum cleaner.

In this tool there is also an air purifier which is activated manually not with a microcontroller. This air purifier source connection is supplied by an AC voltage of 220 generated by a DC to AC inverter. The connection needed for this tool is supplied by 2 batteries in parallel to produce a 24 Volt DC voltage needed to lift or run the PG45 motor. This 24V voltage is reduced by two step downs to 12V to supply the inverter and 9V to activate the power while the power of three IBT-2 is supplied directly by the 5V pin.

D. Testing

Figure 4 shows a block diagram of a Bersaudara Robot system. This robot uses a PG45 24VDC motor, BTS 7960 as a motor driver, sensor input, vacuum cleaner output, air purifier, and Arduino to develop the system. The operation of the sister robot will be based on taking data from a series of inputs that will tell the condition of the space around the hospital patient room. These inputs include ultrasonic, limit switch sensor, and digital compass. Each of these sections will be described in more detail later in the documentation. The data from this input will be entered into a chip which through its software program will decide which direction the robot should move by sending a control signal to the driving motor.

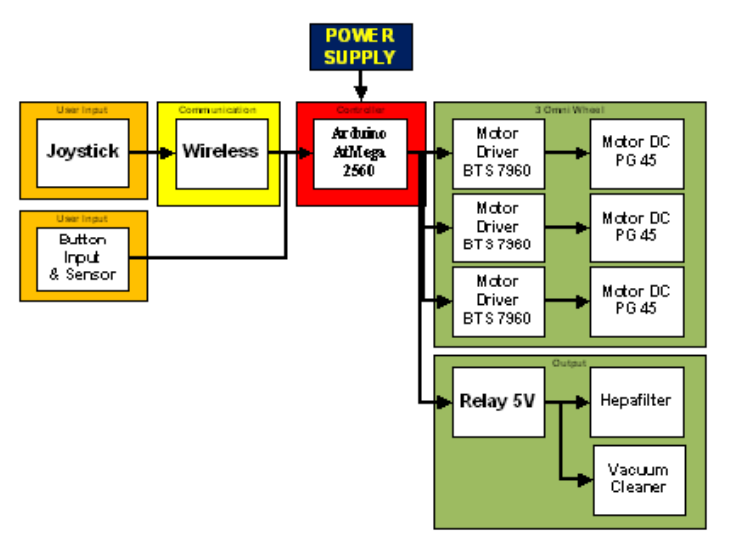


Figure 3. Block diagram of BERSAUDARA robot

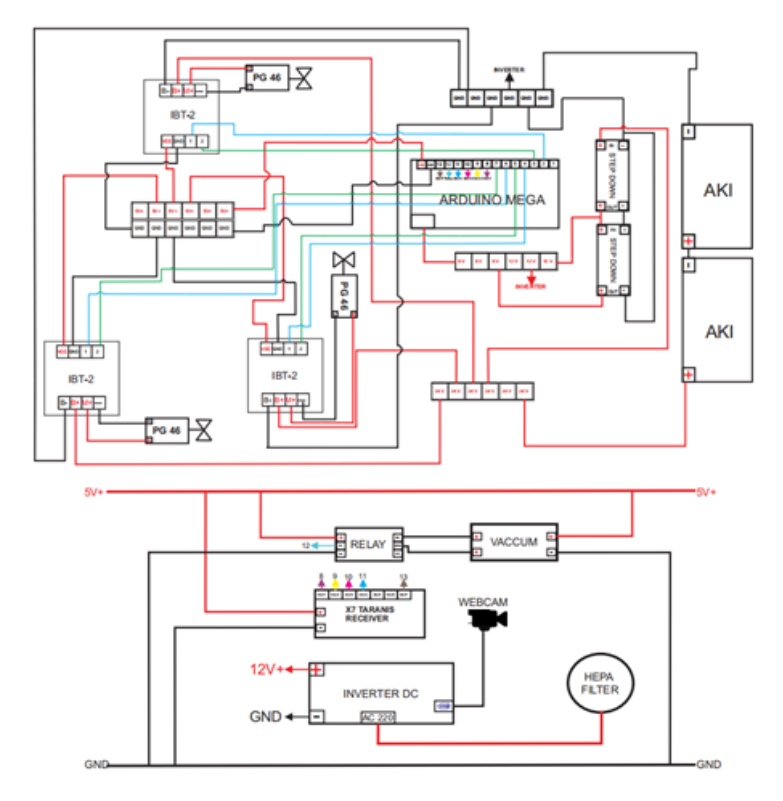


Figure 4. Robot Wirings

The wiring circuit in Figure 4 uses a voltage source from a 12 volt dc lippo battery to supply the controller system, from sensor input, controller and dc motor output. There is an inverter to convert the 12 volt dc voltage to 220 volts to supply the air purifier and webcam camera. for floor cleaning using a voltage of 12 volts dc.

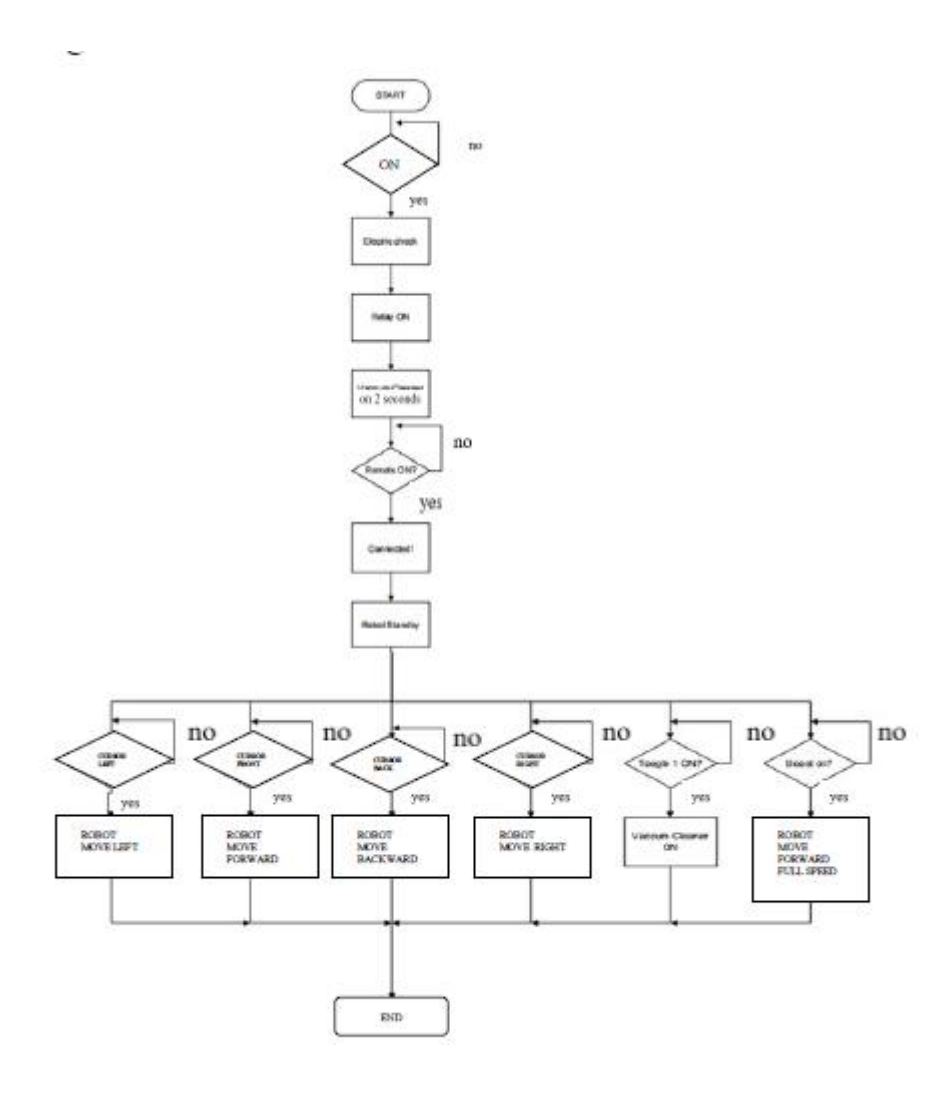


Figure 5. Flowchart

In this research I used a manual wireless controller, so we only need to press the push navigation button on the Playstation 2 wireless controller and the robot is controlled manually with a remote to bring the robot closer to or in front of the door of the COVID-19 patient room with a camera guide located above the robot. When it arrives in front of the patient's room, the robot will switch to automatic mode, will turn on the floor cleaner and air purifier, the robot will automatically enter the room itself to clean the room and air until it reaches every corner of the room. after that the robot will return to the door again.

E. Configuration and Analysis

The results of the analysis of the needs of the floor cleaning robot system developed include:

- a. Robot can work with maneuvering in all directions with the conditions of various shapes of the room.
- b. Robots that are built have a cleaning system in the form of polishing machines and vacuum cleaners.
- c. The robot motor operates with a 24V DC voltage.
- d. Minimum battery voltage of 12 V with a current of 20Ah
- e. Wireless control is needed to reach in all directions.

The hardware and software design developed in the floor cleaning robot includes the design of locating the drive wheel, vacuum cleaner motor and air purifier equipped with UV Sterilizer and HEPA Filter. It also developed the design of wireless communication devices between robots and joystick. Robot drive wheel consists of three motors that form a triangular configuration. The motor is placed at the end of the triangle to move the angle of the omni wheel, so it is easy to move. The design of the placement of the robot motor is shown in Figure 10.

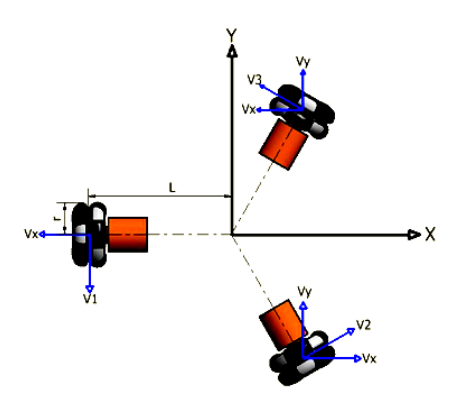


Figure 6. The design of robot's wheels placement

The results of the placement of the wheel design are also used as a reference to place a vacuum cleaner. The placement of the vacuum motor is placed on the back or base of the triangle from where the wheels are placed. A vacuum cleaner is placed in front of so that the floor is free of dust before being polished by. The results of the placement of the motor wheel, motor vacuum cleaner and second floor polisher motor are shown in Figure 2.



Figure 7. The design of the vacuum motors

E1. Human Control Mode

System function tests and floor cleaning robot movements are performed via remote RC based control application input. The test is carried out on the basis of the robot's navigation movement that is forward, backward, right and left shear and motor pole activation.

Table 1. Test Manual Robot

Button re-	Action	Test			
mote		1st	2st	3st	4st
Forward	Robot	OK	OK	OK	OK
Backward		OK	OK	OK	OK
Right		OK	OK	OK	OK
Left		OK	OK	OK	OK
Turn Right		OK	OK	OK	OK
Turn Left		OK	OK	OK	OK

E2. Automatic Mode

The next mode of the system operation is automatic mode of operation. Under automatic mode of operation, the robot can perform all the operations autonomously without any human support to do the needful.

A map-based robot navigation system consisting of mapping, localization, path planning, and trajectory tracking is implemented on a wheeled robot with a Robot Operating System (ROS) platform. To perform the navigation, the robot is equipped with sensors and controllers that can be applied according to the task.



Figure 8. The movement of the vacuum motors



Figure 9. The movement of the vacuum motors

Map Building

In the previous section, we mentioned the design autonomous BERSAUDARA robots used, as well as configuring environment in which the simulation will take place. On this section will describe the algorithm that used in the process of building maps in order to solve navigation problems on robots autonomy, particularly in localization issues.

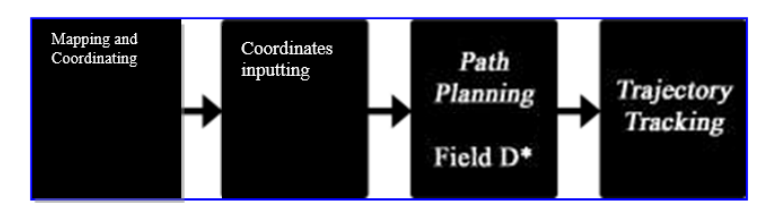


Figure 10. Map-Based Indoor Navigation Process Block Diagram

PATIENT ROOM PATIENT BED WARDROBE

Figure 11. Patient room Maze

Flood Fill Algorithm Rules

- 1. The space in which the mobile robot moves must be represented by a discrete world, from a matrix of two dimensions. This matrix must have the cells (nodes) of the same robot size, so that it can only reach a node traveling a distance equal to its dimensions.
- 2. The body of the robot is used as reference to print the location of the other cells in the whole image, which, in the case of Fig. 11, is generated a matrix array of 5x6 cells.
- 3. Obstacles are in the junctions of the nodes, so there is no one inside a cell. bed patient and wardrobe
- 4. The Bersaudara robot can only make linear movements on the horizontal and vertical axis. So the solution to a path will correspond to the union of orthogonal lines

The robot will be programmed to follow the node whose value increases, if there is an obstacle, the robot will detect the obstacle in front, the ultrasonic sensor will be placed in front of the robot face.

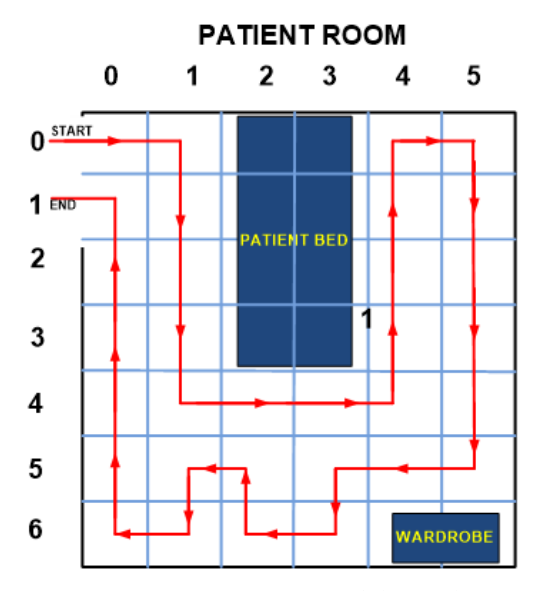


Figure 12. Patient room labyrinth

When the robot is placed back at the starting point, it autonomously navigates towards the destination cell using the optimized path information

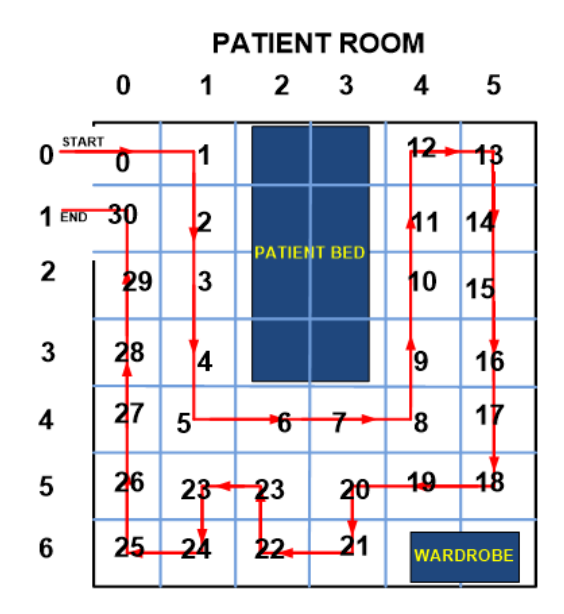


Figure 13. Patient Room plan and movement route robot Bersaudara

After reaching the goal the last flooding occurs and the shortest path linking the starting point with the goal from the mapped part of the maze is determined as shown in Figure 12. The maze flooding is based on the flood fill algorithm which block diagram is shown in Figure 13.

3. Conclusion

The COVID-19 virus is mostly transmitted through droplets and aerosols that stick to the floor of a room and can remain infectious on surfaces at room temperature for several days. Therefore, this robot can be applied in hospitals for COVID-19 patients. The air purifier inside the robot reduces pollutants in the room and improves air quality and is available The UV-C Germicide lamp kills germs, bacteria and viruses trapped in the filter

The design of the room and air cleaning robot has been successfully created and can function properly. Development of a simple floodfill algorithm that can be quickly implemented regardless of mapping and destination search algorithms can be applied in BERSAUDARA robots.

Future work may include studying larger rooms, the ability to solve the best path in a wider and more complex obstacle. This also needs to be further improved specifications object sensors, such as a wide laser range finder, for better.

Acknowledgements

This work was supported by Universitas Sanata Dharma Yogyakarta.

References

- 1. Kementerian Kesehatan RI, Direktorat Jenderal Pencegahan dan Pengendalian Penyakit (P2P). (2020). Pedoman Pencegahan dan Pengendalian Coronavirus Disease (COVID-19). J
- 2. Han Y, Yang H. The transmission and diagnosis of 2019 novel coronavirus infection disease (COVID-19): A Chinese perspective. J Med Virol. 2020; published online March 6. DOI: 10.1002/jmv.25749
- 3. van Doremalen N, Bushmaker T, Morris DH, Holbrook MG, Gamble A, Williamson BN, et al. Aerosol and Surface Stability of SARS-CoV-2 as Compared with SARS-CoV-1. N Engl J Med. 2020; published online March 17. DOI: 10.1056/NEJMc2004973
- 4. Ong SWX, Tan YK, Chia PY, Lee TH, Ng OT, Wong MSY, et al. Air, Surface Environmental, and Personal Protective Equipment Contamination by Severe Acute Respiratory Syndrome Coronavirus 2 (SARS-CoV-2) From a Symptomatic Patient. JAMA. 2020; published online March 4. DOI: 10.1001/jama.2020.3227
- 5. Keputusan menteri kesehatan Republik Indonesia Nomor HK HK.01.07/MENKES/328/2020, tentang panduan pencegahan dan pengendalian corona virus disiese 2019 di tempat kerja perkantoran dan industri dalam mendukung keberlangsungan usaha pada situasi pandemic.
- 6. Kementerian Riset dan Teknologi. (2020). Katalog Inovasi Karya Peneliti dan Perekayasa Kemenristek/BRIN untuk Mengatasi Pandemi. Jakarta: Kementerian Riset dan Teknologi.

Article

Machine Predictive Maintenance by Using Support Vector Machines

Idrus Assagaf 1*, Jonri Lomi Ga 2, Agus Sukandi 1, Abdul Azis Abdillah 1, Samsul Arifin 3

- ¹ Department of Mechanical Engineering, Politeknik Negeri Jakarta, Depok 16425, Indonesia
- ² Department of Mechanical Engineering, University of Birmingham, Birmingham, United Kingdom
- ³ Department of Mathematics, Universitas Bina Nusantara, Indonesia
- * Correspondence: idrus.assagaf@mesin.pnj.ac.id

Abstract: Predictive Maintenance (PdM) is an adoptable worth strategy when we deal with the maintenance business, due to a necessity of minimizing stop time into a minimum and reduce expenses. Recently, the research of PdM is now begin in utilizing the artificial intelligence by using the machine data itself and sensors. Data collected then analyzed and modelled so that the decision can be made for the near and next future. One of the popular artificial intelligences in handling such classification problem is Support Vector Machines (SVM). The purpose of the study is to detect machine failure by using the SVM model. The study is using database approach from the model of Machine Learning. The data collection comes from the sensors installed on the machine itself, so that it can predict the failure of machine function. The study also to test the performance and seek for the best parameter value for building a detection model of machine predictive maintenance The result shows based on dataset AI4I 2020 Predictive Maintenance, SVM is able to detect machine failure with the accuracy of 80%.

Keywords: Predictive Maintenance; SVM; Machine Failure; AI.

Citation: Assagaf, I.; Sukandi, A.; Abdillah, A.A.; Arifin, S. Machine Predictive Maintenance by Using Support Vector Machines. *RiesTech* **2023**, *1*, 2.

https://doi.org/00.000/xxxxx

Academic Editor: Iwan Susanto

Received: 10 September 2022 Accepted: 7 November 2022 Published: 1 January 2023

Publisher's Note: MBI stays neutral with regard to jurisdictional claims in published maps and institutional affiliations.



Copyright: © 2023 by the authors. Licensee MBI, Jakarta, Indonesia. This artilcle is an open acess article distributed under MBI license (https://mbi-journals.com/licenses/by /4.0/).

1. Introduction

Predictive Maintenance (PdM), used to say as "on-line monitoring", "risk-based maintenance" or "condition-based maintenance", is recently a common topic of many research papers. It refers to a smart monitoring system to avoid future failure. Predictive Maintenance have evolved from its initial concept into an automation methods using artificial intelligence based on pattern recognition, machine learning, neural networking and fuzzy logic etc. Automation methods give more proper solutions to many industries which continuously 24/7 detect and collect information which human's eye or ear cannot do. With the combination of integrated sensors, predictive maintenance can be carried out in avoiding unnecessary part replacement, reducing stop time, root cause analysis also saving expenses and improve efficiency.

Predictive Maintenance have overlapping tendency with the concept of preventive maintenance on its activity scheduling. The difference with conventional preventive maintenance is that the activity schedule of predictive maintenance is based on the data collection from sensor and algorithm analysis [1]. Predictive Maintenance have two main focuses: energy efficiency improvement (energy saving focus) and the decrease of unscheduled stop time. Related studies with the predictive maintenance are 1) method and equipment innovation in energy evaluation [2], 2) condition system monitoring include machine failure detection, with many various artificial intelligence techniques [3], [4].

One popular approach taken in predictive maintenance is database approach. It is so called data mining or machine learning approach which is using historical data to study the system behavior model. This model-based approach has capability in combining the physical understanding of the target product and relies on the analytical model that represent the system. Many studies have been done recently, [1], [3]–[7]. However not all data can utilize existing machine learning so that the potentiality of various machine learning methods utilization is so widely open. On of the famous method in classifying is the method of Support Vector Machines (SVM).

The article present PdM methodology based on machine learning. PdM purpose is to early detect the machine failure using artificial intelligence. Model used is SVM. The study use database approach with Machine Learning model sourced from sensors installed in the machine. The study also measures machine learning performance used and seeking the best parameters can be used for building a detection model in its predictive machine maintenance.

2. Materials and Experiment Methods

Support Vector Machine

Experimental method used is Support Vector Machine (SVM). SVM is an algorithm of machine learning to analyze data for classification and linear regression. SVM is a controlled learning method which observe data and sort them into one of two categories. It produces data map sorted out with a safety margin. SVM used when we want to categorize text, picture classification, handwriting recognition and other science applications.

Main goals of SVM algorithm are to categorize every new data input. It makes SVM a linier nonbinary classifier. SVM Algorithm supposed not to just put an object into a category, but also networking a safety wide margin between them in graphics.

SVM implemented in many classification fields, see Fig [8], [9], medics [10], [11], engineering [12], [13] etc. SVM gives good accuracy in many applied fields, so it become one of the popular classification methods. In this study, the author conducted machine failure detection using SVM method and observe the performance result.

Dataset

Dataset used in the study is the open data sourced from UCI Machine Learning titled dataset AI4I 2020 Predictive Maintenance [3], [4], [14]. This dataset composed of 10.000 data point stored as rows within 14 features in columns. In the research we restrict the data used. The study utilizes 6000 data with low type. 5 (five) features used in the study which are ambient temperature (K), process temperature (K), rotation velocity (RPM), the torque (Nm) and wear and tear ability (min) with the classification target number 0 and 1, where 1 is a symbol to describe machine failure. Comes into attention is unequal amount between 0 and 1 target which lead us to utilize under sampling data.

The details related to the features used in the study are as follows:

- 1. Product ID: consist of letter L, M, or H for low (50% of all products), medium (30%) and high (20%) as the variable of product quality and serial product number.
- 2. Ambient temperature [K]: occurred from random walk process normalized to a deviation standard 2 K, defined as 300 K.
- 3. Process temperature [K]: produced from scattered process normalized to a deviation standard 1 K, added to the ambient temperature by 10 K.
- 4. Rotasi velocity [rpm]: measured from 2860 W, covered by normal distribution noise.

- 5. Torque [Nm]: normal distributed torque value approx. 40 Nm with = 10 Nm dan no negative values.
- 6. Wear and tear [min]: Quality variant H/M/L by adding 5/3/2 minutes wear and tear of tools used in process And
- 7. Labelling 'machine failure' which sign whether the machine fail or not in some point for a certain failure mode If at least one of failure modes is true, the failure process and the labelling is set to 1 or vice versa.

3. Results and Discussion

The study explores 2 (two) parameters in building classification model using SVM, which are C and Gamma parameter. The parameter pair tested is C = [0.1,1,10,100,1000] and gamma = [1,0.1,0.01,0.001,0.0001]. Every experiment done by pairing between related C and gamma so that every experiment has combined 25 parameter pairs. The study then seeks for the best pairs. The experiment repeated 5 (five) times for the best accuracy.

Table 1 and Fig 1 describe the result of the experiment. Best average accuracy of 5 experimentation comes from C parameter = 1000 dan Gamma parameter = 0.0001 with the level of accuracy amount of 90%. On the contrary, the lowest average of accuracy comes from parameter value of 1 dan 0.0001 for C dan Gamma. The level of accuracy is only 83%.

Table 1. Expe	riment result or	dataset AI4	I 2020 Predictive	Maintenance ty	pe this is a table.

Experiment	С	Gamma	Accuracy	Accuracy	Average of
Experiment	C	Gaillilla	Training Data	Testing Data	Accuracy
1	1000	0.0001	0.97	0.88	0.93
2	100	0.0001	0.94	0.83	0.89
3	10	0.0001	0.94	0.81	0.88
4	1000	0.0001	0.98	0.85	0.92
5	1	0.0001	0.87	0.78	0.83

We can see from Figure 1 machine failure detected on data AI4I using SVM method on data training reach the peak on 4th experiment with the value of 98% the followed by experiment 1st with the value of 97% dan 5th experiment with the value of 87%. Along with the data trend the accuracy of data testing also sequenced in a same pattern, except in experiment 1st dan 4th whereas data testing from 1st exceeding the 4th by 3%. This is a figure. Schemes have a different format. If there are more than one panel, they should be listed as follows: (a) description of what is in the first panel; (b) description of what is in the second panel. Figures should be placed near the first time they are cited in the main text. A single-line caption should be centered.

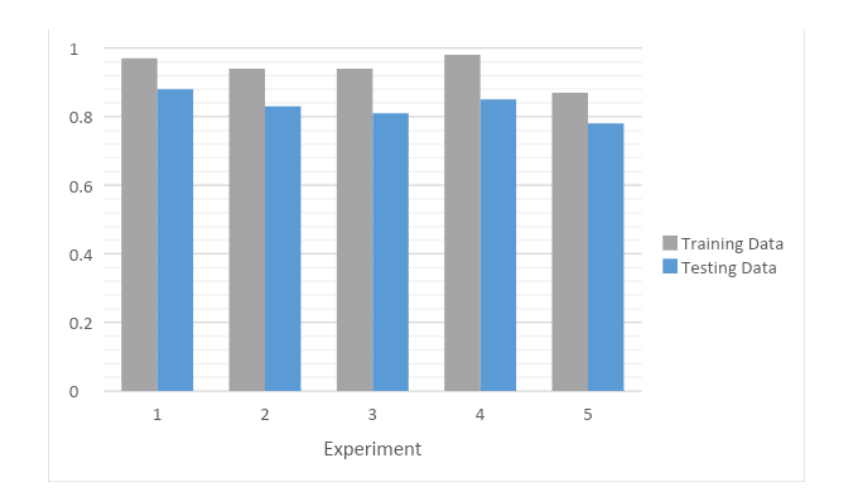


Figure 1. The result of machine failure detection on dataset AI4I 2020 Predictive Maintenance type ${\bf L}$

Generally, the overall accuracy result of more than 80% shows that the performance of SVM model is very promising.

4. Conclusions

Based on the experiment result, the best accuracy of all 5 (five) experiment comes from the value of C dan gamma parameters 1000 dan 0.0001 consecutively. While the accuracy model developed for data training is 98% and for data testing is 88%.

In the study, only some part of dataset and just one machine learning model used by the author, which is Support Vector Machines. The study can be extended by testing various machine learning methods such as random forest, neural network, logistic regression et cetera. Besides the study can be developed by using other dataset sourcing from other vehicle or machinery.

References

- M. Paolanti, L. Romeo, A. Felicetti, A. Mancini, E. Frontoni, and J. Loncarski, "Machine Learning approach for Predictive Maintenance in Industry 4.0," 2018 14th IEEE/ASME International Conference on Mechatronic and Embedded Systems and Applications, MESA 2018, Aug. 2018, doi: 10.1109/MESA.2018.8449150.
- H. Rahman, A. A. Abdillah, A. Apriana, D. Handaya, and I. Assagaf, "Indoor CO2 Level-Based Occupancy Estimation at Low-Scale Occupant using Statistical Learning Method," Proceedings -2021 4th International Conference on Computer and Informatics Engineering: IT-Based Digital Industrial Innovation for the Welfare of Society, IC2IE 2021, pp. 496–499, 2021, doi: 10.1109/IC2IE53219.2021.9649072.
- 3. A. Torcianti and S. Matzka, "Explainable Artificial Intelligence for Predictive Maintenance Applications using a Local Surrogate Model," Proceedings 2021 4th International Conference on Artificial Intelligence for Industries, AI4I 2021, pp. 86–88, 2021, doi: 10.1109/AI4I51902.2021.00029.
- 4. S. Matzka, "Explainable Artificial Intelligence for Predictive Maintenance Applications," Proceedings 2020 3rd International Conference on Artificial Intelligence for Industries, AI4I 2020, pp. 69–74, Sep. 2020, doi: 10.1109/AI4I49448.2020.00023.
- M. Paolanti, L. Romeo, A. Felicetti, A. Mancini, E. Frontoni, and J. Loncarski, "Machine Learning approach for Predictive Maintenance in Industry 4.0," 2018 14th IEEE/ASME International Conference on Mechatronic and Embedded Systems and Applications, MESA 2018, Aug. 2018, doi: 10.1109/MESA.2018.8449150.

- 6. M. D. Dangut, Z. Skaf, and I. K. Jennions, "Handling imbalanced data for aircraft predictive maintenance using the BACHE algorithm," Appl Soft Comput, p. 108924, May 2022, doi: 10.1016/J.ASOC.2022.108924.
- 7. J. Antunes Rodrigues, J. Torres Farinha, M. Mendes, R. Mateus, and A. Marques Cardoso, "Short and long forecast to implement predictive maintenance in a pulp industry," Eksploatacja i Niezawodność, vol. Vol. 24, no. 1, pp. 33–41, 2022, doi: 10.17531/EIN.2022.1.5.
- 8. D. R. S, B. Setyono, and T. Herdha, "Bullet Image Classification using Support Vector Machine," in Journal of Physics: Conference Series, 2016.
- G. Birare and V. A. Chakkarwar, "Automated Detection of Brain Tumor Cells Using Support Vector Machine," 2018 9th International Conference on Computing, Communication and Networking Technologies, ICCCNT 2018, Oct. 2018, doi: 10.1109/ICCCNT.2018.8494133.
- 10. S. Huang, N. Cai, P. P. Pacheco, S. Narrandes, Y. Wang, and W. Xu, "Applications of support vector machine (SVM) learning in cancer genomics," Cancer Genomics Proteomics, vol. 15, no. 1, pp. 41–51, 2018.
- 11. K. Menaka and S. Karpagavalli, "Breast Cancer Classification using Support Vector Machine and Genetic Programming," IJIRCCE, vol. 1, no. 7, pp. 1410–1417, 2013.
- B. Lenz and B. Barak, "Data Mining and Support Vector Regression Machine Learning in Semiconductor Manufacturing to improve virtual metrology," Proceedings of the Annual Hawaii International Conference on System Sciences, pp. 3447–3456, 2013, doi: 10.1109/HICSS.2013.163.
- 13. G. A. Susto, A. Schirru, S. Pampuri, D. Pagano, S. McLoone, and A. Beghi, "A predictive maintenance system for integral type faults based on support vector machines: An application to ion implantation," IEEE International Conference on Automation Science and Engineering, pp. 195–200, 2013, doi: 10.1109/COASE.2013.6653952.
- 14. "UCI Machine Learning Repository: AI4I 2020 Predictive Maintenance Dataset Data Set." https://archive.ics.uci.edu/ml/datasets/AI4I+2020+Predictive+Maintenance+Dataset (accessed May 11, 2022). Author 1, A.B.; Author 2, C.D. Title of the article. *Abbreviated Journal Name* Year, *Volume*, page range.